Crystal structure evolution and superconductivity of the ternary hydride CSH$_3$ under pressure

Kai Hu ,[1] Qingjun Tong,[1] Li-Min Guan,[1] Dahui Wang,[2,*] and Jinqing Yu[1,†]

[1]*School of Physics and Electronics, Hunan University, Changsha 410082, China*
[2]*State Key Laboratory of Laser Interaction with Matter, Northwest Institute of Nuclear Technology, Xi'an 710024, China*

Under high-pressure conditions, the changes of atomic arrangement and stacking of the lattice structures lead to enhanced electronic correlation effect and even superconductivity. Motivated by a recent experimental demonstration of pressure-induced superconductivity in a C-S-H system, in this work, we construct a CSH$_3$ system via simple combining of H$_3$S and C to study the crystal structural evolution and possible superconductivity at high pressure using first-principles calculations. We predicted the trigonal and orthorhombic crystal structures of CSH$_3$ under pressure, with the space groups *R*-3*m*, *Pbcm*, and *Pmmn*, respectively. We find that the trigonal *R*-3*m* phase transform to the orthorhombic *Pbcm* phase at 210 GPa, at which the volume of CSH$_3$ phases drops by ∼7%. Due to large the electronic density of states of the H component near the Fermi level, the T_c is higher in the *Pbcm* and the *Pmmn* phases than in the *R*-3*m* phase. A T_c as high as 98 K is found for the *Pbcm* phase at 250 GPa.

I. INTRODUCTION

The pursuit of high-T_c or room-temperature superconductivity has been a major challenge in physics for decades. The mechanism of conventional superconductors can well be described by the Bardeen-Cooper-Schrieffer (BCS) theory, in which the attraction between electrons is mediated by electron-phonon interaction [1,2]. As the metal hydrides have strong electron-phonon interactions, it is widely believed to be a potential room-temperature superconductor. Previous reports indicate that the metal hydrides have high-T_c properties at relatively low pressures [3]. Additionally, previous studies show that dense carbides isostructural with hydrides have structural stability on decompression due to their rigid carbon sp^3 frameworks, as well as exhibiting high-T_c behavior [4].

In the past 20 years, researchers have paid great attention to high-temperature superconducting hydrides [5]. In 2014, a theoretical study reported that H$_3$S phases were regarded as candidate crystal structures for high-pressure superconducting hydrogen-rich sulfur hydride [6]. Based on the research of H$_3$S, the high-temperature superconducting systems of the ternary hydride include H$_3$SXe (space group *Pm*-3*m*, $T_c = 89$ K) [7], H$_6$SSe (space group *Pm*-3*m*, $T_c = 195$ K) [8], and YSH$_6$ (space group *P*4$_2$/*mmc*, $T_c = 95$ K) [9] have been reported. Furthermore, it has been shown that high-T_c superconductivity can be obtained in other ternary hydrogen compounds such as KScH$_{12}$ (space group *C*2/*m*, $T_c = 122$ K) [10], GaAsH$_6$ (space group *Pm*-3, $T_c = 98$ K) [10], CH$_4$Mg (space group *P*4/*nmm*, $T_c = 84$ K) [11], and LiPH$_6$ (space group *Pm*-3, $T_c = 150$ K) [12]. The ternary hydride materials with relatively low T_c such as Li$_5$MoH$_{11}$ (space group

P6$_3$*cm*, $T_c = 6.5$ K) [13], BaReH$_9$ (space group P6$_3$/*mmc*, $T_c = 7$ K) [14], and CH$_4$K (space group P2$_1$/*m*, $T_c = 12$ K) [15] have also been discovered. Recently, it was reported that the high-temperature superconductors can be realized via CH$_4$ intercalated H$_3$S-like hydride at high pressure [16,17]. Another four metastable phases were uncovered in CS$_2$H$_{10}$, and one of the metastable phases, the *Cmc*2$_1$ phase, has a high T_c of 155 K at 150 GPa [18]. Based on synchrotron x-ray diffraction studies, Bykova *et al.* [19] and Lamichhane *et al.* [20] found that the denser carbon-bearing S-H phases may be formed in the C-S-H system under pressure. In particular, it has been experimentally reported that the C-S-H ternary system can achieve room-temperature superconductivity at high pressure [21]. Ge *et al.* [22] also researched the effects of hole doping on the superconductivity of H$_3$S with the *Im*3*m* structure at megabar pressures. And the hole doping can fine-tune the Fermi energy to reach the electronic density-of-states peak maximizing the electron-phonon coupling [22]. The above theoretical and experimental results also stimulate us to search for high T_c in the ternary system. Based on our interest in the theoretical research of the C-S-H ternary system, considering the complexity of the C-S-H ternary system and the limited calculation sources, we combined H$_3$S with C to form the CSH$_3$ system by the simplest way, to predict the crystal structures and corresponding superconductivity. Additionally, we also studied the full components of the C$_x$SH$_3$ ($x = 2$–4) system at high pressures, and the calculation results indicate that those compounds are metastable phases.

In this paper, using the crystal structure prediction technology and first-principles calculations, we found three stable structures for CSH$_3$ ternary hydride at 100, 200, and 300 GPa, i.e., the *R*-3*m*, *Pbcm*, and *Pmmn* phases. The enthalpy calculation results indicate that the *R*-3*m* phase of CSH$_3$ transforms to the *Pbcm* phase at 210 GPa. Under compression, the

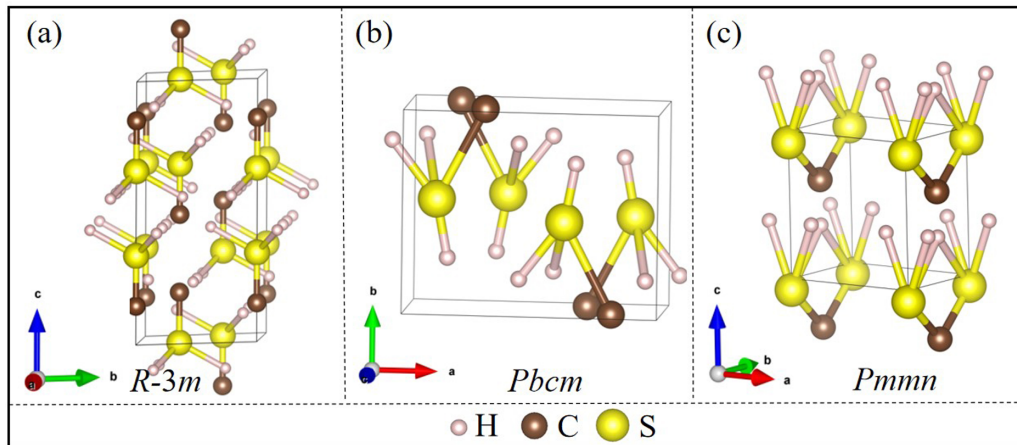*wangdahui@nint.ac.cn
†jinqing.yu@hnu.edu.cn

FIG. 1. The crystal structures of CSH_3 for (a) the high-pressure trigonal phase (space group R-$3m$), (b) the high-pressure orthorhombic phase (space group $Pbcm$), and (c) the high-pressure orthorhombic phase (space group $Pmmn$). The small pink, brown, and large yellow balls represent H, C, and S atoms, respectively.

enthalpy difference between the $Pmmn$ phase and the $Pbcm$ phase is getting smaller. At above 270 GPa, H_3S ($R3m$) [6] and C (diamond) [23] are more energetically competitive than CSH_3. However, comparing with the enthalpy of the phases of CSH_3, C (diamond) [23] +S ($I4_1/bcd$) [24] +3H ($C2/c$) [25] are not energetically favorable under pressure. Remarkably, the T_c of the $Pbcm$ phase in CSH_3 is 98 K at 250 GPa. Our work may provide a possible way to seek high T_c of the C-S-H ternary system in the future.

II. COMPUTATIONAL METHODS

CALYPSO [26], which uses local structural optimization techniques to minimize the local lattice energy, is employed for the computations. It can generate random structures symmetrically constrained within 230 space groups [27]. Once a particular space group is selected, the lattice parameters are then confined within the chosen symmetry. In the particle swarm optimization scheme, a structure (an individual) is regarded as a particle, and a set of individual structures is called a population. The lattice parameters (unit cell) of new structures are the same as that of the previous generation. The CSH_3 simulation cells ranging in 1–4 formula units and the full components of the C_xSH_3 ($x = 2$–4) system within 2–4 formula units were performed with the CALYPSO structure prediction method at 100, 200, and 300 GPa. Computations were carried out with a population size of 30 structures per generation up to 50 generations, and stopped after the generation of 1300–1500 structures. The structural relaxations and total-energy calculations were performed in the framework of density-functional theory, as implemented in the Vienna *ab initio* simulation package (VASP) [28]. The interactions of electrons and ions can be described by the generalized gradient approximation with the Perdew-Burke-Ernzerhof functional [29] and the projector augmented wave method [30]. The phonon dispersions were calculated with the supercell approach [31], which is implemented in the PHONOPY code [32]. The cutoff energy of the plane wave basis was set to 550 eV and the k-point resolution was $2\pi \times 0.03$ Å^{-1}. For each ionic relaxation, the maximum force of the atoms is less

than 0.01 eV/Å. Based on the density-functional perturbation theory (DFPT) [33], the electron-phonon coupling (EPC) parameter λ was calculated by the QUANTUM ESPRESSO package [34]. The cutoff energy was set to 80 Ry for the H, S, and C elements with suitable convergence. In the calculations of EPC for the R-$3m$, $Pbcm$, and $Pmmn$ phases of CSH_3, the k meshes were $16 \times 16 \times 16$, $8 \times 16 \times 16$, and $16 \times 16 \times 16$, while the q meshes were $4 \times 4 \times 4$, $2 \times 4 \times 4$, and $4 \times 4 \times 4$, respectively.

III. RESULTS AND DISCUSSION

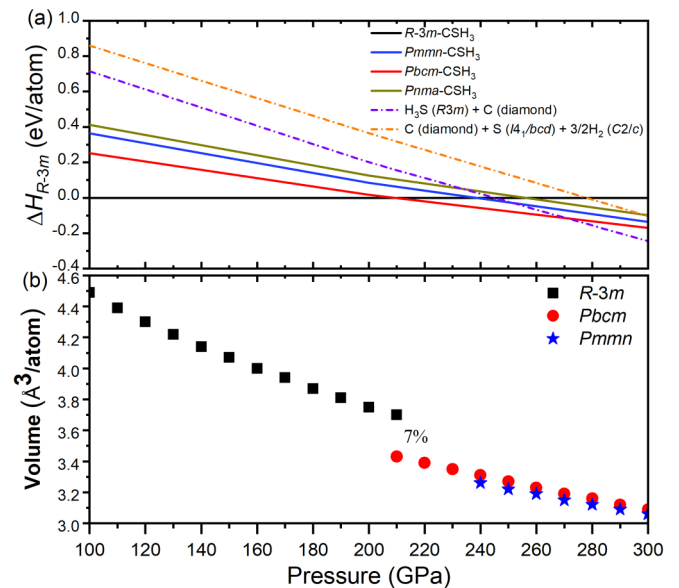At high pressure, we predicted the structures for the trigonal phase (space group R-$3m$), the orthorhombic phase

FIG. 2. (a) The relative enthalpy as a function of pressure with the R-$3m$ phase as a reference. (b) The volume variation as a function of pressure for the R-$3m$, $Pbcm$, and $Pmmn$ phases. At the transition pressures of 210 GPa, the $Pbcm$ phase shows 7% volume decrease.

TABLE I. Structural information for CSH_3 phases, including the space group, cell parameters, and Wyckoff positions.

Space group	Pressure (GPa)	Lattice parameters (Å)	Wyckoff position
R-$3m$	100	$a = b = 4.292; c = 8.447$ $\alpha = \beta = 90°; \gamma = 120°$	H: $18h$ $(-0.199, -0.397, 0.435)$ S: $6c$ $(0,0,0.661)$ C: $6c$ $(0,0,0.852)$
$Pbcm$	250	$a = 4.492; b = 5.607; c = 2.593$ $\alpha = \beta = \gamma = 90°$	H: $4d$ $(-5/6, 0.947, 1.250)$ H: $4d$ $(-0.828, 0.442, 1.250)$ H: $4d$ $(-0.263, 1/3, 3/4)$ S: $4d$ $(-0.450, 0.877, 3/4)$ C: $4d$ $(-0.004, 0.691, 3/4)$
$Pmmn$	250	$a = 3.487; b = 2.546; c = 3.634$ $\alpha = \beta = \gamma = 90°$	H: $4f$ $(0.821, 1, -0.261)$ H: $2b$ $(1, 1/2, -0.691)$ S: $2a$ $(1/2, 1/2, -0.924)$ C: $2b$ $(1/2, 1, -0.617)$

(space group $Pbcm$), and the orthorhombic phase (space group $Pmmn$) of CSH_3, and plotted them in Fig. 1. In the trigonal R-$3m$ phase of CSH_3, a sulfur atom forms bonds surrounding by three hydrogen atoms to build a tetrahedron. It is interesting to see that the R-$3m$ phase transforms to the $Pbcm$ phase with the H-S tetrahedron, and the $Pmmn$ phase has similar H-S tetrahedron at high pressure, as drawn in Fig. 1. The H-S bond lengths of the H_3S phases are between 1.39 and 1.84 Å [6], which are close to the H-S bond length of the three CSH_3 phases (1.68 Å for R-$3m$; 1.31, 1.61, and 1.84 Å for $Pbcm$; and 1.77 and 1.89 Å for $Pmmn$ phases at 100, 250, and 250 GPa, respectively).

Figure 2(a) shows the enthalpy differences of high-pressure phases for CSH_3 with respect to the R-$3m$ phase at the pressure range of 100–300 GPa. It can be seen that the trigonal R-$3m$ phase transforms to an orthorhombic $Pbcm$ phase at 210 GPa, an orthorhombic $Pmmn$ phase occurs at 240 GPa,

and the enthalpy difference between the $Pmmn$ phase and the $Pbcm$ phase decreases with the enhencement of pressure. When the pressure is higher than 270 GPa, the H_3S and C are more energetically favorable than CSH_3 as indicated by the enthalpy pressure curves. We also found that the enthalpy of C (diamond) [23] +S ($I4_1/bcd$) [24] +3H ($C2/c$) [25] are not competitive compared with the phases of CSH_3 at high pressure. The volume of the $Pbcm$ phase is compressed by about 7% compared with the volume of the R-$3m$ phase at the transition pressure of 210 GPa, as shown in Fig. 2(b). The lattice parameters and Wyckoff positions for these CSH_3 phases are presented in Table I. Figure S1 of the Supplemental Material shows the enthalpy differences of high-pressure phases for C_xSH_3 ($x = 2$–4) with respect to the $P1$ phase at the pressure range of 100–300 GPa [35]. The phonon spectra calculation results show that those compounds are dynamically unstable at high pressure, as shown in Figs. S2(b) and S2(c) of the
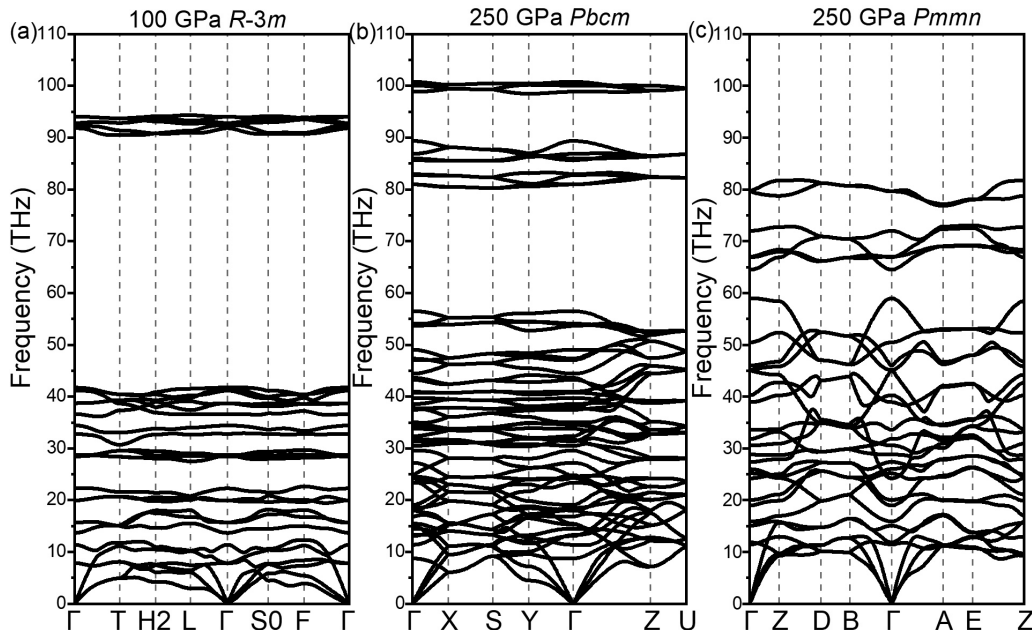
FIG. 3. The phonon band structures of (a) the R-$3m$ phase at 100 GPa, (b) the $Pbcm$ phase at 250 GPa, and (c) the $Pmmn$ phase at 250 GPa.
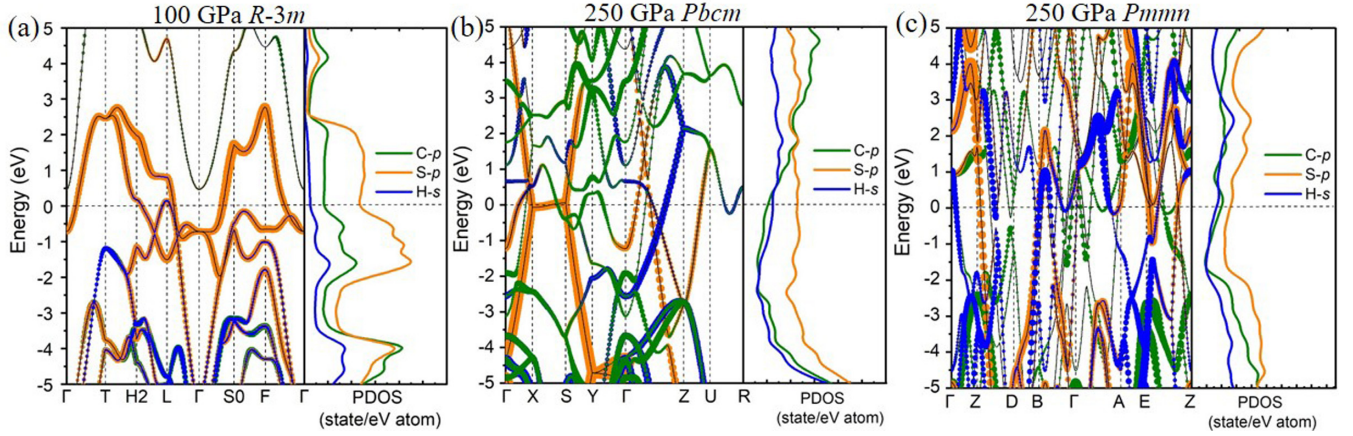
FIG. 4. The electronic band structure and corresponding DOS for (a) the *R-3m* phase at 100 GPa, (b) the *Pbcm* phase at 250 GPa, and (c) the *Pmmn* phase at 250 GPa.

Supplemental Material. The structural information of the C_2SH_3, C_3SH_3, and C_4SH_3 compounds at high pressure is listed in Table SI of the Supplemental Material.

In order to verify the dynamic stability of the CSH_3 phases, we plot the phonon dispersion curves in Fig. 3. The calculation results suggest that the *R-3m*, *Pbcm*, and *Pmmn* phases of CSH_3 are dynamically stable at 100, 250, and 250 GPa, respectively. Figure S2(a) of the Supplemental Material shows the phonon band structure of the *Pnma* phase, which is dynamically unstable at 250 GPa. The vibration frequency of the optical branch of the *Pbcm* phase is higher than that of the *Pmmn* phase as illustrated in Figs. 3(b) and 3(c), which indicates that the interaction between the C and H atoms for the *Pbcm* phase is stronger than that of the *Pmmn* phase at 250 GPa in the CSH_3 system. The calculated Raman modes show that the Raman intensities of the *Pbcm* and *R-3m* phases are stronger than that of the *Pmmn* phase at the high-frequency range of 2500–$3400\,\mathrm{cm}^{-1}$, as shown in Fig. S3 of the Supplemental Material.

The relevant electronic band structures and the corresponding projection electronic density of states (DOS) of the CSH_3 phases are illustrated in Fig. 4. From Fig. 4, one can see that the *R-3m*, *Pbcm*, and *Pmmn* phases of CSH_3 are metallic with the bands across the Fermi levels, and these bands are mainly contributed by H-s, S-p, and C-p orbitals. For the *R-3m* phase, the Fermi level is mainly contributed by the S-p orbital (marked by orange) with one large electronic pocket between the points H_2 and L. Due to the strengthening of the interaction between atoms for the *Pbcm* phase, there is a flat band near the Fermi level along the $X \rightarrow S$ direction at 250 GPa. From the DOS diagram in Fig. 4(a), one can see that the S-p electrons occupy the main contribution in the Fermi level. At the low energy region below the Fermi level (-4 eV), the S-p electrons with the same spin orientation strongly hybridize with the C-p electrons, resulting in the formation of one DOS peak due to large orbital overlapping. Under pressure, the H electrons are more involved in coupling to contribute the states around the Fermi level as drawn in Figs. 4(b) and 4(c). Due to the small distribution of the electronic states of H near the Fermi level, the T_c of the *R-3m* phase is relatively low. When the phase transition occurs, the contribution of H

electrons for the *Pbcm* phase and the *Pmmn* phase around the Fermi level increases, which may lead to an increase of T_c at high pressure.

To further understand the atomic bonds of the CSH_3 phases, the corresponding projected two-dimensional (2D) electronic localization functions (ELFs) are shown in Fig. 5. The ELF was previously proposed by Becke and Edgecombe to measure electron pairing by defining $\mathrm{ELF} = (1 + \chi_\sigma^2)^{-1}$, where $\chi_\sigma = D_\sigma/D_\sigma^0$, and $D_\sigma = \tau_\sigma - (\nabla \rho_\sigma)^2/4\rho_\sigma$, $D_\sigma^0 = \frac{3}{5}(6\pi^2)^{2/3}\rho_\sigma^{5/3}$, $\tau_\sigma = \sum_i^\sigma |\nabla \varphi_i|^2$, where D_σ^0 corresponds to a uniform electron gas with spin density, τ_σ is the positive-definite kinetic-energy density [36]. The ELF values are defined as 1, 0.5, and close to 0, indicating strong electrons, electron gas, and nonelectron localizations, respectively. As illustrated in Fig. 5, the ELF values of the H atoms are approaching 1, exhibiting strong covalent bonding characteristics. The S and C atoms are connected with weak covalent bonding at high pressure.

Based on the framework of the BCS phonon-mediated pairing mechanism [1,37], the superconducting properties of the CSH_3 phases were calculated by the Allen-Dynes modified McMillan equation [38].

$$T_C = f_1 f_2 \frac{\omega_{\log}}{1.2} \exp\left[-\frac{1.04(1+\lambda)}{\lambda - \mu^*(1+0.62\lambda)}\right], \quad (1)$$

where f_1 and f_2 are the strong coupling and shape correction factors, respectively, defined as

$$f_1 = \sqrt[3]{1 + \left[\frac{\lambda}{2.46(1+3.8\mu^*)}\right]^{3/2}}, \quad (2)$$

$$f_2 = 1 + \frac{\left(\frac{\bar{\omega}_2}{\omega_{\log}} - 1\right)\lambda^2}{\lambda^2 + \left[1.82(1+6.3\mu^*)\left(\frac{\bar{\omega}_2}{\omega_{\log}}\right)\right]^2}. \quad (3)$$

The logarithmic average frequency $\omega_{\log}$, mean square frequency $\bar{\omega}_2$, and EPC constant λ were given by

$$\omega_{\log} = \exp\left[\frac{2}{\lambda} \int \ln(\omega) \frac{\alpha^2 F(\omega)}{\omega} d\omega\right] \quad (4)$$
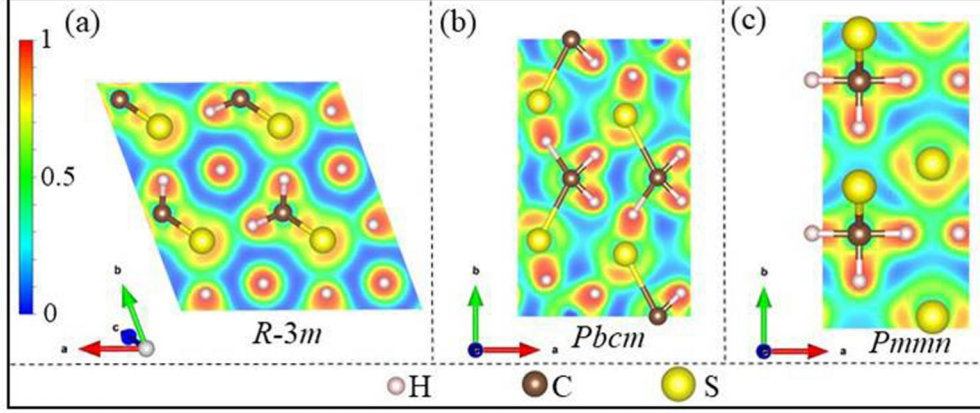
FIG. 5. The 2D ELF CSH$_3$ for (a) the R-$3m$ phase in the (0 0 1/2) plane, (b) the $Pbcm$ phase in the (0 0 1) plane, and (c) the $Pmmn$ structure in the (0 0 1) plane. The small pink, gray, and large yellow balls are H, C, and S atoms, respectively.

$$\bar{\omega}_2 = \sqrt{\frac{2}{\lambda} \int \alpha^2 F(\omega) \omega \, d\omega}, \tag{5}$$

$$\lambda = 2 \int \frac{\alpha^2 F(\omega)}{\omega} d\omega. \tag{6}$$

The typical value of the Coulomb pseudopotential was set to $\mu^* = 0.10$ (0.13) [39]. The EPC constant λ, logarithmic frequency $\omega_{\log}$, mean square frequency $\bar{\omega}_2$, and superconducting critical temperature T_c [37,40] for these CSH$_3$ phases are listed in Table II. For the $Pbcm$ phase, the T_c approximates 98 K ($\mu^* = 0.13$, 87 K) with the $\omega_{\log} = 877.0$ and $\lambda = 1.31$ at 250 GPa, which was higher $T_c = 63$ K ($\mu^* = 0.13$, 53 K) of the $Pmmn$ phase at 250 GPa. Previous study has reported that the T_c of H$_3$SXe at 240 GPa is 89 K [7], which is smaller than our calculation result. Figure 6 shows the phonon band structure, phonon DOS, Eliashberg spectral function $\alpha^2 F(\omega)$, and EPC constant λ of the $Pbcm$ phase. Due to the much larger mass of the S atom than that of the H atom and the C atom, the frequencies below 30 THz are dominated by the vibrations of S atoms, and 20–40 THz are contributed by C atoms, while above 30 THz are mainly contributed by H atoms, as shown in Fig. 6(b). Interestingly, ∼80% of λ is contributed by the acoustical phonon with the vibrational frequencies below 20 THz, especially for the acoustical phonon modes near the Γ point in the q space, as drawn in Figs. 6(a) and 6(c). The above results suggest that the enhancement of T_c originates from the pressure-increased EPC. In the Supplemental Material, Figs. S4 and S5 also show the phonon band structures, phonon DOS, Eliashberg spectral function $\alpha^2 F(\omega)$, and EPC constant λ of the R-$3m$ phase and the $Pmmn$ phase at 100 and 250 GPa, respectively. The frequencies below 10 THz (15 THz) are dominated by the vibrations of S atoms, and 10–35 THz (15–30 THz) are contributed by C atoms, while above 35 THz (30 THz) are mainly contributed by H atoms for the R-$3m$ phase ($Pmmn$ phase). Compared with the R-$3m$ phase and the $Pmmn$ phase, the vibration of H atoms in the $Pbcm$ phase contribute to the high-frequency range than the former.

IV. CONCLUSIONS

Using crystal structure prediction and first-principles calculations, we predicted the structure evolution of the CSH$_3$ phases at high pressure. Our calculations exhibit that the R-$3m$ phase will transform to the $Pbcm$ phase at 210 GPa.

TABLE II. Superconductivity of CSH$_3$ at pressures calculated using the Allen-Dynes modified McMillan equation.

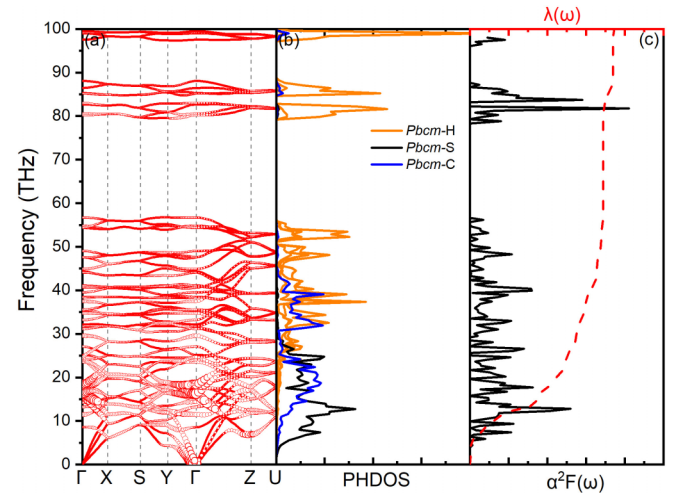| Phase	Pressure (GPa)	λ	$\omega_{\log}$ (K)	$\bar{\omega}_2$ (K)	T_c (K) $\mu^* = 0.10$	$\mu^* = 0.13$
R-$3m$	100	1.81	224.4	658.8	36	33
	150	0.47	389.1	1555.5	4	2
$Pbcm$	250	1.31	887.0	1441.0	98	87
$Pmmn$	250	0.93	940.4	1566.2	63	53

FIG. 6. (a) Phonon band structure, with the radius of the circles proportional to the strength represents the phonon linewidth, (b) atomically resolved phonon DOS, and (c) Eliashberg spectral function $\alpha^2 F(\omega)$ and electron-phonon coupling constant λ for the orthorhombic $Pbcm$ phase at 250 GPa.

The enthalpy of H_3S and C is more energetically favorable than CSH_3 at above 270 GPa. The T_c of the *Pbcm* phase and the *Pmmn* phase is higher than that of the *R*-3*m* phase, owing to the larger electronic states of H distribution near the Fermi level in the former cases. Interestingly, the calculation results indicate that the phases of the C_xSH_3 ($x = 2$–4) system are metastable. The predicted superconductivity of the CSH_3 phases at high pressure provides a possible way to seek high T_c of the C-S-H ternary system in the future.

[1] J. Bardeen, L. N. Cooper, and J. R. Schrieffer, Phys. Rev. **108**, 1175 (1957).

[2] N. W. Ashcroft, Phys. Rev. Lett. **21**, 1748 (1968).

[3] N. W. Ashcroft, Phys. Rev. Lett. **92**, 187002 (2004).

[4] S. Y. Lu, H. Y. Liu, I. I. Naumov, S. Meng, Y. W. Li, J. S. Tse, B. Yang, and R. J. Hemley, Phys. Rev. B **93**, 104509 (2016).

[5] H. Wang, X. Li, G. Y. Gao, Y. W. Li, and Y. M. Ma, WIREs Comput. Mol. Sci. **8**, e1330 (2018).

[6] D. F. Duan, Y. X. Liu, F. B. Tian, D. Li, X. L. Huang, Z. L. Zhao, H. Y. Yu, B. B. Liu, W. J. Tian, and T. Cui, Sci. Rep. **4**, 6968 (2014).

[7] D. Li, Y. Liu, F. B. Tian, S. L. Wei, Z. Liu, D. F. Duan, B. B. Liu, and T. Cui, Front. Phys. **13**, 137107 (2018).

[8] B. B. Liu, W. W. Cui, J. M. Shi, L. Zhu, J. Chen, S. Y. Lin, R. M. Su, J. Y. Ma, K. Yang, M. L. Xu *et al.*, Phys. Rev. B **98**, 174101 (2018).

[9] X. W. Liang, S. T. Zhao, C. C. Shao, A. Bergara, H. Y. Liu, L. Y. Wang, R. X. Sun, Y. Zhang, Y. F. Gao, Z. S. Zhao *et al.*, Phys. Rev. B **100**, 184502 (2019).

[10] T. Ishikawa, T. Miyake, and K. Shimizu, Phys. Rev. B **100**, 174506 (2019).

[11] F. B. Tian, D. Li, D. F. Duan, X. J. Sha, Y. X. Liu, T. Yang, B. B. Liu, and T. Cui, Mater. Res. Express **2**, 046001 (2015).

[12] Z. J. Shao, D. F. Duan, Y. B. Ma, H. Y. Yu, H. Song, H. Xie, D. Li, F. B. Tian, B. B. Liu, and T. Cui, npj Comput. Mater. **5**, 104 (2019).

[13] D. Meng, M. Sakata, K. Shimizu, Y. Iijima, H. Saitoh, T. Sato, S. Takagi, and S. Orimo, Phys. Rev. B **99**, 024508 (2019).

[14] T. Muramatsu, W. K. Wanene, M. Somayazulu, E. Vinitsky, D. Chandra, T. A. Strobel, V. V. Struzhkin, and R. J. Hemley, J. Phys. Chem. C **119**, 18007 (2015).

[15] J. X. Han, H. Zhang, and G. H. Zhong, Int. J. Mod. Phys. C **30**, 1950061 (2019).

[16] W. W. Cui, T. G. Bi, J. M. Shi, Y. W. Li, H. Y. Liu, E. Zurek, and R. J. Hemley, Phys. Rev. B **101**, 134504 (2020).

[17] Y. Sun, Y. F. Tian, B. W. Jiang, X. Li, H. F. Li, T. Iitaka, X. Zhong, and Y. Xie, Phys. Rev. B **101**, 174102 (2020).

[18] M. Y. Du, Z. H. Zhang, T. Cui, and D. F. Duan, Phys. Chem. Chem. Phys. **23**, 22779 (2021).

[19] E. Bykova, M. Bykov, S. Chariton, V. B. Prakapenka, K. Glazyrin, A. Aslandukov, A. Aslandukova, G. Criniti, A. Kurnosov, and A. F. Goncharov, Phys. Rev. B **103**, L140105 (2021).

[20] A. Lamichhane, R. Kumar, M. Ahart, N. P. Salke, N. Dasenbrock-Gammon, E. Snider, Y. Meng, B. Lavina, S. Chariton, V. B. Prakapenka *et al.*, J. Chem. Phys. **155**, 114703 (2021).

[21] E. Snider, N. Dasenbrock-Gammon, R. McBride, M. Debessai, H. Vindana, K. Vencatasamy, K. V. Lawler, A. Salamat, and R. P. Dias, Nature (London) **586**, 373 (2020).

[22] Y. F. Ge, F. Zhang, R. P. Dias, R. J. Hemley, and Y. G. Yao, Mater. Today Phys. **15**, 100330 (2020).

[23] S. L. Qiu, Eur. Phys. J. B **87**, 147 (2014).

[24] O. Degtyareva, E. Gregoryanz, M. Somayazulu, H. K. Mao, and R. J. Hemley, Phys. Rev. B **71**, 214104 (2005).

[25] C. J. Pickard and R. J. Needs, Nat. Phys. **3**, 473 (2007).

[26] Y. C. Wang, J. Lv, L. Zhu, and Y. M. Ma, Comput. Phys. Commun. **183**, 2063 (2012).

[27] Y. C. Wang, J. Lv, L. Zhu, and Y. M. Ma, Phys. Rev. B **82**, 094116 (2010).

[28] G. Kresse and J. Furthmülle, Phys. Rev. B **54**, 11169 (1996).

[29] J. P. Perdew, K. Burke, and M. Ernzerhof, Phys. Rev. Lett. **77**, 3865 (1996).

[30] P. E. Blochl, Phys. Rev. B: Condens. Matter **50**, 17953 (1994).

[31] K. Parlinski, Z. Q. Li, and Y. Kawazoe, Phys. Rev. Lett **78**, 4063 (1997).

[32] A. Togo, F. Oba, and I. Tanaka, Phys. Rev. B **78**, 134106 (2008).

[33] S. Baroni, S. de Gironcoli, and A. D. Corso, Rev. Mod. Phys. **73**, 515 (2001).

[34] P. Giannozzi, S. Baroni, N. Bonini, M. Calandra, R. Car, C. Cavazzoni, D. Ceresoli, G. L. Chiarotti, M. Cococcioni, I. Dabo *et al.*, J. Phys.: Condens. Matter **21**, 395502 (2009).

[35] See Supplemental Material at http://link.aps.org/supplemental/10.1103/PhysRevB.105.094108 for enthalpy differences, phonon band structures, and structural information of the C_xSH_3 ($x = 2$–4) compounds, as well as Raman modes, phonon band structures, phonon density of states, Eliashberg spectral function, and electron–phonon coupling constant of the CSH_3 phases.

[36] A. D. Becke and K. E. Edgecombe, J. Chem. Phys. **92**, 5397 (1990).

[37] F. Giustino, Rev. Mod. Phys. **89**, 015003 (2017).

[38] P. B. Allen and R. C. Dynes, Phys. Rev. B **12**, 905 (1975).

[39] D. Belitz, Phys. Rev. B **35**, 1651 (1987).

[40] J. Bardeen and D. Pines, Phys. Rev. **99**, 1140 (1955).